Seismic Evidence for an Earthquake Nucleation Phase

W. L. Ellsworth and G. C. Beroza

Near-source observations show that earthquakes initiate with a distinctive seismic nucleation phase that is characterized by a low rate of moment release relative to the rest of the event. This phase was observed for the 30 earthquakes having moment magnitudes 2.6 to 8.1, and the size and duration of this phase scale with the eventual size of the earthquake. During the nucleation phase, moment release was irregular and appears to have been confined to a limited region of the fault. It was characteristically followed by quadratic growth in the moment rate as rupture began to propagate away from the nucleation zone. These observations suggest that the nucleation process exerts a strong influence on the size of the eventual earthquake.

In order for an earthquake to occur, a fault must evolve from a locked state to one in which slip occurs at speeds of up to several meters per second and propagates along the fault at a rupture velocity of several kilometers per second. The abrupt onset of *P* waves emanating from an earthquake's hypocenter has generally been interpreted as evidence for self-similar rupture growth from the beginning of the earthquake. Dynamic solutions for self-similar models of crack growth at a constant stress drop lead to far-field velocity seismograms that grow linearly from the arrival time of the initial *P* wave (Fig. 1A) (*1*). However, recent observations of velocity seismograms indicate that the initiation of rupture commonly violates the self-similar assumption (*2*). This violation commonly appears as an interval of weak ground motion that precedes the strong ground motion of the main event and has sometimes been described as an immediate foreshock (*3*, *4*). We found this behavior at the beginning of earthquakes that span eight orders of magnitude in seismic moment (Table 1). In this report, we quantify the temporal evolution of this process and suggest two possible interpretations.

W. L. Ellsworth, U.S. Geological Survey, Menlo Park, CA 94025, USA.
G. C. Beroza, Department of Geophysics, Stanford University, Stanford, CA 94305, USA.

We used near-source, digital recordings of the hypocentral *P* wave to study the early stages of earthquakes (Table 1 and Fig. 2). The velocity seismograms exhibit a range of behavior. In some cases, such as events 1 and 10, the velocity seismogram is one-sided but returns to zero before growing rapidly. In other cases, such as events 4 and 16, the velocity seismograms do not return to zero before they begin to grow dramatically. In no case do the data in Fig. 2 exhibit a linear increase of velocity in time measured from the initiation of the earthquake. A similar observation has been made for microearthquakes (moment magnitude $M_w < 2.7$) in Japan (*2*).

The recent Northridge, California, earthquake, $M_w = 6.7$, is an example for which there have been multiple observations of the

Table 1. Moment rate functions used to derive parameters determined with a *P*-wave velocity $V_P = 6$ km s^{-1}, $V_P/V_S = 1.73$, and $\mu = 30{,}000$ MPa for a surface receiver at a radial distance, *R*, from the hypocenter. Letters following the date identify aftershocks of the Northridge, California, earthquake (N); earthquakes located near Anza, California (A); mine tremors recorded underground in South Africa (M); earthquakes at Parkfield, California, recorded in the 1-km-deep Varian borehole (P); and earthquakes in Long Valley Caldera, California, recorded in the 2-km-deep Long Canyon borehole (L). The total duration of the earthquake is the duration of the seismic nucleation phase, ν, plus the time from breakaway until the cessation of seismic radiation, τ. The seismic moment release during nucleation phase, M_o^ν, is given as a percent of the main shock moment, M_o. Computations of the nucleation zone radius, r_ν, and dynamic stress drop during breakaway, $\Delta\sigma_b$, are described in the text. We assume a rupture velocity $V = 0.8\ V_S$ in the determination of $\Delta\sigma_b$.

Event	Date	M_W	M_o (N−m)	*R* (km)	ν (s)	τ (s)	M_o^ν (%)	r_ν (m)	$\Delta\sigma_b$ (MPa)
1	19 Sep 1985	8.1	1.4×10^{21}	25	5.0	50	0.2	6300	5.0
2	28 Jun 1992	7.3	9×10^{19}	21	3.0	20	0.4	3400	4.1
3	25 Apr 1989	6.9	2.4×10^{19}	27	0.53		0.02	850	3.4
4	18 Oct 1989	6.9	2.8×10^{19}	25	1.6	9	1.6	2200	1.9
5	17 Jan 1994	6.7	1×10^{19}	19	0.5	6	0.2	600	40
6	15 Oct 1979	6.5	6×10^{18}	19	0.59	15	0.6	1000	14
7	9 Jun 1980	6.4	4.8×10^{18}	13	0.44		0.02	410	6.0
8	24 Oct 1993	6.4	5.8×10^{18}	46	0.36		0.03	520	5.5
9	28 Jun 1992	6.2	2×10^{18}	29	0.46		0.16	560	8.1
10	23 Apr 1992	6.1	1.4×10^{18}	44	0.12	4	0.01	150	17
11	31 May 1990	5.9	7.5×10^{17}	24	0.082	1.7	0.04	130	64
12	29 Jun 1992	5.8	4.8×10^{17}	27	0.46	1.7	0.1	420	2.9
13	28 Jun 1991	5.5	2.8×10^{17}	23	0.34	0.8	1.6	480	18
14	20 Mar 1994N	5.3	8.9×10^{16}	22	0.127	0.87	1.31	230	42
15	3 Dec 1988	4.9	2.4×10^{16}	16	0.11	0.8	1.4	220	15
16	16 Jan 1993	4.9	2.4×10^{16}	29	0.21	0.8	2.2	300	8.8
17	14 Nov 1993	4.8	2.0×10^{16}	15	0.20	0.3	0.8	410	1.1
18	11 Aug 1993	4.7	1.3×10^{16}	10	0.73	0.45	3.0	270	8.3
19	3 Feb 1994N	4.2	2×10^{15}	26	0.047	0.26	0.43	73	9.6
20	6 Feb 1994N	4.1	1.4×10^{15}	24	0.026	0.3	0.13	46	8.0
21	2 Feb 1994N	3.8	5×10^{14}	17	0.039	0.27	0.30	66	2.3
22	27 Oct 1991A	3.7	3.5×10^{14}	15	0.038	0.10	0.6	52	6.5
23	6 Feb 1994N	3.7	3.5×10^{14}	23	0.030	0.32	0.25	36	8.3
24	26 Oct 1992P	3.6	2.5×10^{14}	11	0.022	0.05	1.8	28	100
25	1 Feb 1994N	3.6	2.5×10^{14}	11	0.013	0.24	0.10	32	3.4
26	2 Jan 1990A	3.5	1.8×10^{14}	16	0.038	0.11	0.6	39	8.2
27	4 Feb 1994N	3.5	1.8×10^{14}	16	0.008	0.21	0.45	35	8.4
28	8 Mar 1994N	3.4	1.3×10^{14}	22	0.047	0.15	0.71	100	0.4
29	30 Jan 1988M	3.3	8.1×10^{13}	2	0.027	0.17	1	18	60
30	8 Nov 1992L	2.6	7.9×10^{12}	6	0.004	0.03	0.2	11	5.4

initiation process (Fig. 3) (5). At high magnification it is clear that the earthquake started abruptly. It is also clear that this beginning of the earthquake is dwarfed by what follows. At 0.5 s into the event, there was a sharp increase in the ground velocity, corresponding to a 30-fold increase in the seismic moment release in the next 0.5 s (6). We characterize the evolution of the source process by the moment-rate function, $\dot{M}_o(t)$, for an equivalent point source (7).

We define the interval between the initial *P* wave and the sudden increase in growth of the velocity seismogram as the seismic nucleation phase and denote its duration as ν; ν is measured as the time interval between the first arrival and the abrupt increase in moment acceleration (8) (Fig. 4). Although this is a retrospective definition, Fig. 4 shows that there is a sudden and unambiguous increase in the moment acceleration.

Our analysis shows that ν scales as the cube root of the total seismic moment, M_o (Fig. 5). This scaling is suggestive of constant stress-drop scaling observed for earthquakes (9); however, the comparison in Fig. 5 is between the duration of the seismic nucleation phase alone and the moment of the entire earthquake. Despite the correlation, it is not obvious how to interpret ν in terms of source properties because we do not know the rupture velocity. Indeed, models of nucleation predict that rupture will occur in place before propagating away from the nucleation zone (10, 11).

The duration of the nucleation phase, normalized by the duration of the rest of the earthquake, τ, is distinctly long-tailed. There are even a few instances for which ν is comparable to or greater than τ (Table 1). The distribution of ν/τ is approximately log-normal (12) and has a mean value of 0.16. A $1/t$ distribution, which describes the temporal decay of aftershock rates and the temporal growth of foreshock rates, does not fit the observations (13).

The moment released during the seismic nucleation phase

$$M_o^{\nu} = \int_0^{\nu} \dot{M}_o(t)dt \qquad (1)$$

represents only a small fraction of the total seismic moment, averaging 0.5% (Table 1). The fraction of the moment during the seismic nucleation phase shows no systematic variation with the total moment of the earthquake. During nucleation, the character of moment release shows considerable variation; however, for most events it is episodic rather than gradual (Fig. 2) (14, 15).

If we assume that the place at which the earthquake begins has stress and strength

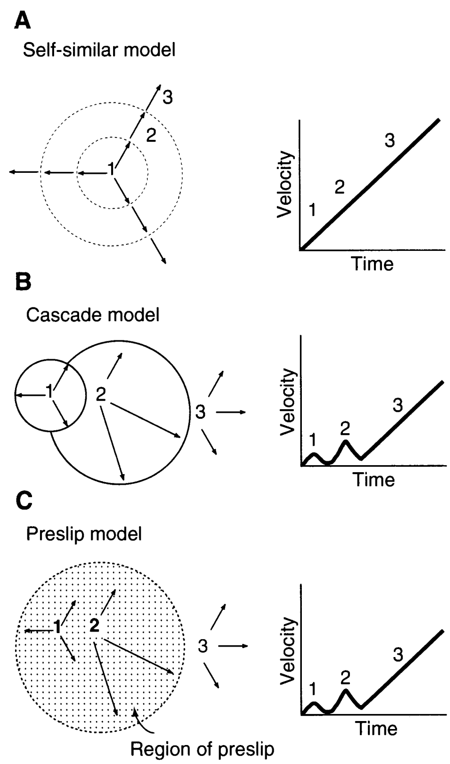

Fig. 1. Three conceptual models of the nucleation process of earthquakes, as viewed on the fault plane, and their corresponding far-field velocity seismograms. The numbers refer to the slip state of the fault at three different episodes during the initial growth stage of the rupture. By time 3, all three models have evolved into a fully dynamic rupture propagating along the fault plane. (**A**) Self-similar growth of the rupture from the instant of initiation leads to linear growth of the far-field velocity seismogram. The observation of the seismic nucleation phase and the abrupt transition to breakaway are clearly inconsistent with this model. (**B**) Cascade model in which the spontaneous occurrence of subevent 1 leads to the delayed failure of area 2, which in turn leads to delayed failure of the remainder of the fault at time 3. (**C**) The start of the earthquake in the preslip model is preceded by aseismic slip in the stippled region. Subevents 1 and 2 are confined within this zone until time 3 when the rupture breaks out of the preparation zone. The velocity seismograms in (B) and (C) are difficult to distinguish in the far field.

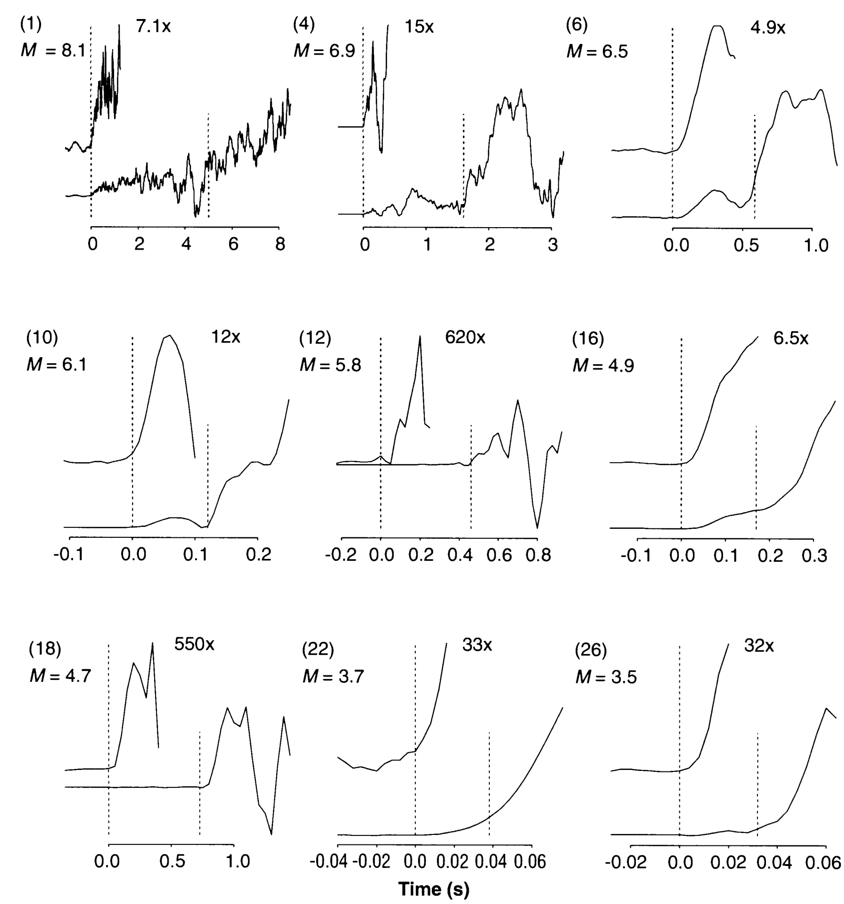

Fig. 2. A representative set of broadband velocity seismograms used in our analysis, shown at two amplitude scales in order to display the character of both the first arrival and the subsequent strong arrivals. The numbers in parentheses refer to the event number in Table 1. Time increases from left to right and is at a different scale for each seismogram. Velocity amplitudes and polarities are normalized. The arrival time of the *P* wave is at zero and is marked by the longest dashed line. Each seismogram is plotted at two amplitude scales with the higher magnification (top) showing the onset of the first *P* wave. The interval between zero and the second dashed vertical line spans the duration, ν, of the seismic nucleation phase. Self-similar growth of the rupture predicts a linear increase in velocity with time, which begins at time ν.

conditions that are grossly similar to the rest of the fault, we can estimate dimensions for and average slip within the nucleation zone. Under this assumption, the stress drop in the nucleation zone will be approximately equal to the dynamic stress drop in the surrounding zone, $\Delta\sigma_b$, that is released when the event begins to grow rapidly. The quantity $\Delta\sigma_b$ is determined in the interval immediately after the seismic nucleation phase according to the relation (16)

$$\dot{M}_o(t) = D(V)\,\Delta\sigma_b\,V^3t^2 \tag{2}$$

where V is the rupture velocity and D is a function that is nearly unity and depends weakly on the rupture velocity. We typically observe quadratic growth of $M_o(t)$ after the nucleation phase, as predicted by Eq. 2, which also can be seen as a linear growth of the velocity seismograms (Figs. 2 and 3). We term this interval of quadratic growth the "breakaway phase." The velocity seismogram will exhibit linear growth only for the initial stages of dynamic rupture until the finite size of the fault, stress, or strength heterogeneities influence subsequent rupture propagation.

We estimated the radius, r_ν, and average fault slip, Δu_ν, of the nucleation zone from the measured quantities $M_o^{\ \nu}$ and $\Delta\sigma_b$ using the equations

$$r_\nu = \left(\frac{7}{16}\frac{M_o^{\ \nu}}{\Delta\sigma_b}\right)^{1/3} \tag{3}$$

and

$$\Delta u_\nu = \frac{M_o^{\ \nu}}{\mu\pi r_\nu^{\ 2}} \tag{4}$$

where μ is the shear modulus. These estimates (Table 1 and Fig. 6) will be applicable as long as the process involves the failure of contiguous areas (17). Our estimate of r_ν should be relatively insensitive to errors in $M_o^{\ \nu}$ or $\Delta\sigma_b$ because it depends on the cube root of those quantities.

Both the fault slip during nucleation and the radius of the nucleation zone scale as the cube root of the main-shock seismic moment (Fig. 6). This scaling follows from the observation that the ratio $M_o^{\ \nu}/M_o$ is independent of M_o and the assumption of matching stress drop. Although $M_o^{\ \nu}$ is a small fraction of M_o, the scaling implies that slip during nucleation is approximately 20% of the slip in the main-shock (18). A simple estimate of the mean rupture velocity during the seismic nucleation phase is given by r_ν/ν for the self-similar crack model and $2r_\nu/\nu$ for unilateral propagation. This yields a low apparent rupture velocity of 1.5 km s^{-1} for radial expansion. Events of the tail of the log-normal distribution have low apparent rupture velocities under either assumption (19).

The duration, seismic moment, source dimension, and average slip of the process that generates the seismic nucleation phase all scale with the moment of the eventual earthquake, suggesting that the ultimate size of an earthquake is strongly influenced by the nucleation process. We suggest two contrasting models that may explain these observations.

One interpretation, which we call the cascade model, is that there is no difference between the beginnings of large and small earthquakes (20, 21). A large earthquake results when a small earthquake triggers a cascade of increasingly larger slip events (Fig. 1B). In this case, the seismic nucleation phase represents a stochastic accumulation of small events that occur from the initiation of the first event until the largest subevent.

In the cascade model, the scaling between $M_o^{\ \nu}$, r_ν, Δu_ν, and M_o could arise if rupture propagation is controlled by a hierarchical distribution of fault elements (21). In this model, rupture continues to grow if it can cause successively larger fault elements to fail. The last jump in the size of fault elements determines the size of the earthquake and would be identified with the breakaway phase. Thus, the scaling is controlled by the breakaway phase rather than by the seismic nucleation phase. The timing of the successive failure in this hierarchy would have to satisfy the observations on the distribution of ν. A mechanism (22) needs to be imposed to account for delayed failure.

Another interpretation, which we call the preslip model, is that the beginnings of small and large earthquakes differ (Fig. 1C).

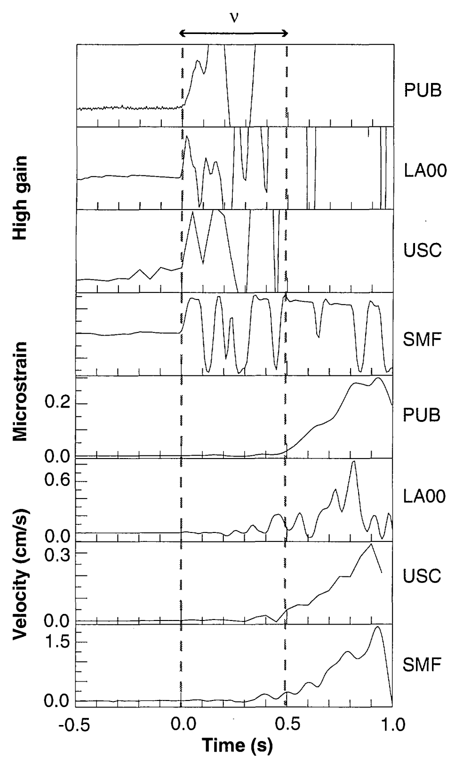

Fig. 3. Near-source recordings of the initial *P* waves from the hypocenter of the 17 January 1994 Northridge earthquake at four sites. The top traces display seismograms at high magnification to illustrate impulsive onset at $t = 0$ s. The bottom traces show the full dynamic range of motion during the first second of the earthquake. During the first 0.5 s of the earthquake, the ground motions were weak compared to the next 0.5 s. We identify this interval of weak motions as the seismic nucleation phase of the Northridge earthquake. After 0.5 s the velocity grows linearly, corresponding to a dynamic stress drop of 40 MPa. The stations shown include the borehole strainmeter PUB (Δ = 66 km, azimuth = 68°), digital accelerometer LA00 (Δ = 14 km, azimuth = 145°), broadband seismometer USC (Δ = 32 km, azimuth = 132°), and telemetered geophone (upper trace) and accelerometer (lower trace) station SMF (Δ = 23 km, azimuth = 158°). All traces are shown as ground velocity, except for the dilatational strain at PUB, which is equivalent to the velocity in the plane-wave limit. The polarities of all traces are reversed for comparison with models.

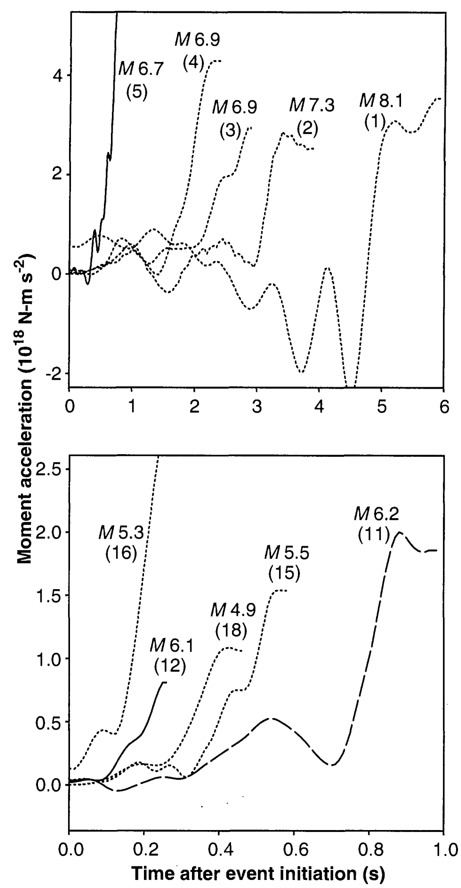

Fig. 4. Moment-acceleration functions for the initiation of earthquakes over a large range of magnitudes. The numbers in parentheses refer to the event numbers in Table 1. Moment acceleration is proportional to the ground velocity in the far-field approximation and was determined by deconvolution of complete synthetic seismograms from observed broadband seismograms. Each earthquake begins weakly and then abruptly accelerates into a large earthquake. The point of transition is identified as the end of the seismic nucleation phase. Before that, the moment acceleration is erratic and sometimes negative, indicating that rupture growth is irregular.

In the preslip model, failure initiates aseismically, with an episode of slow, stable sliding over a limited region that gradually accelerates until the slipping patch reaches a critical size (*23*). The process then becomes unstable, and fracture propagates

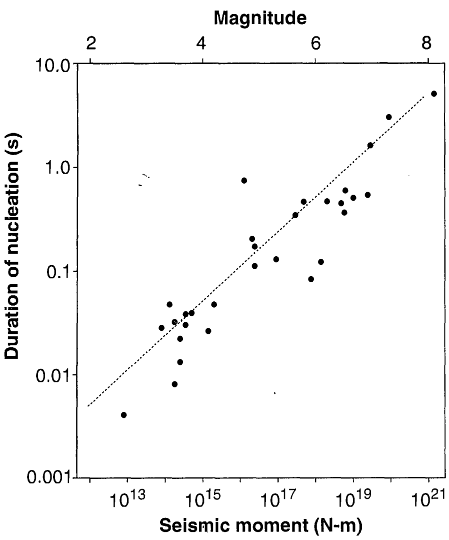

Fig. 5. The seismic moment M_o versus ν. The straight line has a slope of 1/3, indicating a scaling of $M_o \sim \nu^3$.

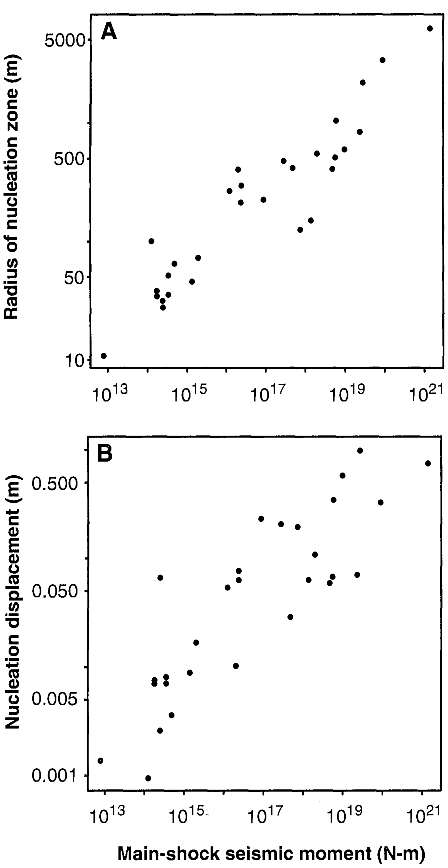

Fig. 6. Relation between r_ν and M_o (**A**) and between Δu_ν and M_o (**B**) derived on the basis of the stress-drop matching assumption.

away from the nucleation zone at high rupture velocity in an earthquake (*24*). The seismic nucleation phase represents the final stages of this process during which rupture is confined to the nucleation zone. Rate- and state-dependent friction models not only lead to the development of an aseismic nucleation zone but also provide a mechanism for rupture delay.

In the preslip model, the scaling between nucleation zone properties and mainshock moment could result from the magnitude of the slip amplitude at breakaway. When this amplitude is large, the resulting dynamic rupture is difficult to stop and a large earthquake results. In simple terms, the earthquake propagates farther and grows larger because it is "pushed harder" at the beginning (*25*). By analogy with laboratory experiments (*11*), the scaling of slip within and the dimension of the nucleation zone may be controlled by the critical displacement (D_c) for the fault surface.

Observations of the seismic nucleation phase for all earthquakes we examined as well as other examples in the literature (*2*, *26*) suggest that such a phase is a common, if not universal, feature of the earthquake nucleation process. Its properties rule out the class of self-similar models for earthquake nucleation, including not only the idealized self-similar shear crack (*1*) but, more generally, any growth process that maintains scale independence (*20*). The fundamental difference between the two interpretations is that in the preslip model the seismic nucleation phase is the culmination of a process already in progress, whereas in the cascade model, the seismic nucleation phase marks the very beginning of the process.

Of the two models developed here, only the preslip model offers any possibility of short-term earthquake prediction. Even if it is correct, the size of the nucleation zone need not scale with earthquake size and might be undetectably small (*27*). Our observations, however, indicate that the seismic nucleation zone scales with the size of the eventual earthquake. For earthquakes $M_w \geq 6.5$, we find that the radius of the nucleation zone ranges from 600 m to 6 km (Table 1). If the zone develops aseismically, its small dimensions and limited deformation arising from aseismic slip within it may be extremely difficult to detect as a strain signal (*15*) but might be large enough to generate other detectable signals (*28*).

REFERENCES AND NOTES

1. In the dynamic solution for a circular earthquake source of constant stress drop expanding at constant rupture velocity [B. V. Kostrov, *J. Appl. Math. Mech.* **28**, 1077 (1964)], the fault area grows quadratically with time and the average slip grows linearly with time, resulting in a seismic moment that grows as the cube of time. Thus, the seismic moment rate grows quadratically with time. Because the far-field displacement pulse is proportional to the moment rate [K. Aki and P. G. Richards, *Quantitative Seismology: Theory and Methods* (Freeman, San Francisco, 1981), p. 81], the far-field velocity seismogram will grow linearly with time.
2. Y. Iio, *Geophys. Res. Lett.* **19**, 477 (1992).
3. The 1979 Imperial Valley earthquake: P. Spudich and E. Cranswick, *Bull Seismol. Soc. Am.* **74**, 2083 (1984); the 1989 Loma Prieta earthquake: D. J. Wald, D. V. Helmberger, T. H. Heaton, *ibid.* **81**, 1540 (1991).
4. The 1978 Izu-Oshima, Japan, earthquake: K. Shimazaki and P. Somerville, *ibid.* **69**, 1343 (1979); the 1987 Superstition Hills earthquake: A. Frankel and L. Wennerberg, *ibid.* **79**, 515 (1989); the 1992 Landers earthquake: R. Abercrombie and J. Mori, *ibid.* **84**, 725 (1994); the 1989 Loma Prieta earthquake: L. Dietz and W. Ellsworth, *U.S. Geol. Surv. Prof. Pap. 1550D*, in press.
5. J. H. Steidl, A. G. Tumarkin, B. H. Chin, *Seismol. Res. Lett.* **65**, 45 (1994); E. Hauksson, K. Hutton, L. Jones, J. Mori, Program for Northridge Abstracts, 89th Annual Meeting of the Seismological Society of America, 5 to 7 April 1994, Pasadena, CA.
6. W. L. Ellsworth and G. C. Beroza, Program for Northridge Abstracts 89th Annual Meeting of the Seismological Society of America, 5 to 7 April 1994, Pasadena, CA.
7. We derive *P*-wave displacement seismograms by integrating the original velocity or acceleration records after correction for instrument response. We assume half-space Green's functions [L. R. Johnson, *Geophys. J. R. Astron. Soc.* **37**, 99 (1974)] and use independently determined fault orientations. The moment-rate function, $M_0(t)$, is determined from the displacement waveforms by deconvolution. We assume that the extent of the source during nucleation is small so that the effects of spatial variations in Green's functions and directivity are negligible compared with effects arising from the time dependence of the slip. Tests of independent recordings of the Northridge earthquake (Fig. 3) yielded nearly identical moment-rate functions, which confirms that our assumptions are appropriate for the early stages of the earthquake. We also obtained similar results for either half-space or layered-media Green's functions.
8. The moment acceleration is obtained by differentiating the moment rate with respect to time. Moment acceleration is proportional to the far-field velocity seismogram.
9. H. Kanamori and D. L. Anderson, *Bull. Seismol. Soc. Am.* **65**, 1073 (1975); R. Abercrombie and P. Leary, *Geophys. Res. Lett.* **20**, 1511 (1993).
10. S. Das and C. H. Scholz, *J. Geophys. Res.* **86**, 6039 (1981).
11. J. H. Dieterich, in *Earthquake Source Mechanics*, S. Das, J. Boatwright, C. Scholz, Eds. (American Geophysical Union, Washington, DC, 1986), pp. 37–47; M. Ohnaka, *Tectonophysics* **211**, 149 (1992); J. H. Dieterich, *ibid.* p. 115.
12. The log-normal distribution arises in systems in which failure occurs at a threshold and growth toward the threshold is randomly proportional to growth that has already occurred. It may be possible to draw an analogy between statistical failure models [J. H. K. Kao, in *Proceedings of the Eleventh National Symposium on Reliability and Quality Control*, Miami, FL, 12 to 14 January 1965 (IEEE, New York, 1965), p. 240] and earthquake nucleation. This analogy is supported by the irregular behavior of the moment-acceleration function during the nucleation phase (Fig. 4), which suggests that the nucleation process is unsteady. Although this behavior might explain why ν follows a log-normal distribution, it does not relate ν to properties of the nucleation zone.
13. The frequency of aftershocks that follow a large earthquake [F. Omori, *J. Coll. Sci. Imp. Univ. Tokyo* **7**, 111 (1894)] and foreshocks that precede an earthquake [L. M. Jones and P. Molnar, *J. Geophys. Res.* **84**, 3596 (1979)] are observed to follow a $1/t$ distribution.
14. Direct observation of a slow nucleation process has been reported in the case of only a few earthquakes [A. M. Dziewonski and F. Gilbert, *Nature* **247**, 185 (1974); I. S. Sacks, S. Suyehiro, A. T. Linde, J. A.

Snoke, *ibid.* **275**, 599 (1978); T. H. Jordan, *Geophys. Res. Lett.* **18**, 2019 (1991); P. F. Ihmlé, P. Harabaglia, T. H. Jordan, *Science* **261**, 177 (1993); P. F. Ihmlé and T. H. Jordan, *ibid.* **266**, 1547 (1994)], and these observations remain controversial [E. A. Okal and R. J. Geller, *Phys. Earth Plant. Inter.* **18**, 176 (1979); S. Kedar, S. Watada, T. Tanimoto, *J. Geophys. Res.* **99**, 17893 (1994).

15. No evidence for a slow nucleation process has been detected in other well-observed events [D. C. Agnew and F. K. Wyatt, *Bull. Seismol. Soc. Am.* **79**, 480 (1989); M. J. S. Johnston, A. T. Linde, M. T. Gladwin, *Geophys. Res. Lett.* **17**, 1777 (1990)]. These observations limit the seismic moment of a slow process to about 0.5% of M_o. Thus, slow release of moment equivalent to M_o^{ν} would be unobservable in most instances.
16. The dynamic stress drop of the event is proportional to the slope of the velocity seismogram [J. Boatwright, *Bull. Seismol. Soc. Am.* **70**, 1 (1980)]. Propagation effects, such as intrinsic attenuation [M. T. Gladwin and F. D. Stacey, *Phys. Earth Planet. Inter.* **8**, 332 (1974)] and forward scattering (T. Mukerji, G. Mavko, D. Mujica, N. Lucet, *Geophysics*, in press) can distort the velocity pulse shape but will be quite small relative to the effects we observe at such short distances.
17. We measure the seismic moment, which is the product of the average slip, the faulted area, and the shear modulus μ (assumed to be 30,000 MPa). Although we use the static solution for a constant stress-drop circular crack ($M_o^{\nu} = 16\Delta\sigma r_{\nu}^3/7$), our estimates of the average slip and the faulted area are not strongly dependent on the circular geometry of the model.
18. See, for example, table 1 of C. H. Scholz [*Bull. Seismol. Soc. Am.* **72**, 1 (1982)].
19. Another observation that supports low mean rupture velocity is the distance between the initial hypocenter and the location of the point of breakaway, which has been determined for only a few earthquakes (*4*). In each of these cases, this distance divided by ν implies an average rupture velocity of 20 to 50% of the shear wave velocity.
20. M. Wyss and J. N. Brune, *Bull. Seismol. Soc. Am.* **57**, 1017 (1967); P. Bak and C. Tang, *J. Geophys. Res.* **94**, 15635 (1989).
21. Y. Fukao and M. Furumoto, *Phys. Earth Planet Inter.* **37**, 149 (1985).
22. A plausible physical mechanism for delayed rupture is provided by the rate and state variable friction law. It is possible to explain the time decay of aftershocks, known as Omori's law, with such a model [J. H. Dieterich, *J. Geophys. Res.* **99**, 2601 (1994)]. This friction law also gives rise to stable preslip as part of the nucleation process.
23. Failure in both crack models [D. J. Andrews, *J. Geophys. Res.* **81**, 5679 (1976)] and frictional models [J. H. Dieterich, *ibid.* **84**, 2161 (1979)] of earthquakes is stable and is confined to a limited region of the fault until a critical dimension is achieved and the stiffness (stress drop per unit fault slip) falls below the critical level [J. R. Rice and J.-C. Gu, *Pure Appl. Geophys.* **121**, 187 (1983)].
24. P. G. Okubo, *J. Geophys. Res.* **94**, 12321 (1989); B. Shibazaki and M. Matsu'ura, *Geophys. Res. Lett.* **19**, 1189 (1992).
25. There is evidence that slip in large earthquakes scales linearly with rupture length [see (*18*)]. It has been proposed that this scaling is caused by the strength of the rupture at initiation [P. A. Bodin and J. N. Brune, personal communication; T. H. Heaton, *Phys. Earth Planet. Inter.* **64**, 1 (1990)]. However, our observations provide the first direct evidence to support this conjecture.
26. Y. Umeda, *Tectonophysics* **175**, 81 (1990); *ibid.* **211**, 13 (1992); M. Ohnaka, *J. Phys. Earth* **41**, 45 (1993).
27. J. H. Dieterich, in *Earthquake Source Mechanics*, S. Das, J. Boatwright, C. Scholz, Eds. (American Geophysical Union, Washington, DC, 1986), pp. 37–47.
28. For example, low-frequency electromagnetic field variations were observed before the 1989 Loma Prieta earthquake [A. C. Fraser-Smith, A. Bernardi, R. A. Helliwell, P. R. McGill, O. G. Villard Jr., *U.S. Geol. Surv. Prof. Pap. 1550-C* (1993), p. C17.

29. We are grateful to J. Dieterich, A. Gusev, T. Hanks, R. Madariaga, J. Rice, P. Segall, W. Thatcher, J. Vidale, and M. Zoback for their comments. We thank J. Brune, Y. Iio, B. Shibazaki, and S. Kedar, who provided preprints of their work. J. Anderson, P. Harben, E. Hauksson, S. Hough, M. Johnston, P. Malin, A. McGarr, G. Simila, J. Steidl, F. Vernon, Y. Zeng, the University of California at Berkeley, California Division of Mines and Geology, Southern California Earthquake Center, and the U.S. Geological Survey provided valuable data. G.C.B. was supported by the Electric Power Research Institute and a National Science Foundation Presidential Young Investigator Award.

15 November 1994; accepted 15 February 1995

Late Triassic Turtles from South America

Guillermo W. Rougier,* Marcelo S. de la Fuente, Andrea B. Arcucci

The discovery of Triassic (Norian) turtles from the northwest part of Argentina extends the South American record of turtles by 60 million years. Two skeletons, one almost complete, represent a new genus and species of a basal turtle, *Palaeochersis talampayensis*. This turtle is a member of the family Australochelidae that was recently erected for *Australochelys africanus* from the Lower Jurassic of South Africa. Here, it is proposed that Australochelidae is the sister group of *Proterochersis* plus Casichelydia, that turtles were diverse by the Late Triassic, and that Casichelydia probably originated during the Jurassic.

Recent findings and restudy of previous collections have led to a new understanding of the origin of Casichelydia (pleurodires and cryptodires) and of turtle relations (*1–8*). A few German localities of Norian age have yielded complete skeletons of *Proganochelys quenstedti* (*7*) and the carapace, plastron, and girdles of *Proterochersis robusta* (*9*). Apart from these fossils, only extremely poor material from the Triassic attributed to *Proganochelys* has been reported worldwide (*10*). *Proterochersis* was previously identified as the oldest pleurodire (*9*). Therefore, pleurodires and cryptodires, the groups that include all living turtles, should have made their appearance during the Upper Triassic (*7, 9, 11*). This would place modern turtles among the wide array of taxa, including frogs, crocodiles, mammals, and dinosaurs, that originated around this time (*12*). On the basis of our fossils, we question the inclusion of *Proterochersis* in Pleurodira and accordingly the Triassic origin of Casichelydia. Here, we report the discovery of two partial turtle skeletons collected from the upper part of the Triassic Los Colorados Formation in northwestern Argentina. These fossils are associated with a tetrapod assemblage of Norian age (*13–15*) and they extend the South American record of turtles by 60 million years (*16*).

G. W. Rougier, Department of Vertebrate Paleontology, American Museum of Natural History, Central Park West at 79th Street, New York, NY 10024-5192, USA, and Consejo Nacional de Investigaciones Científicas y Técnicas (CONICET), Museo Argentino de Ciencias Naturales, Avenida A. Gallardo 470, 1405 Buenos Aires, Argentina.
M. S. de la Fuente, CONICET, Facultad y Museo de Ciencias Naturales de La Plata, Division de Paleontología de Vertebrados, Paseo del Bosque sin número, 1900 La Plata, Argentina.
A. B. Arcucci, Instituto de Antropología, Universidad Nacional de La Rioja, Avenida Ortíz de Ocampo 1700, 5300 La Rioja, Argentina.

*To whom correspondence should be addressed.

Palaeochersis talampayensis gen. nov. sp. nov. is represented by an unusually complete skeleton (Figs. 1 and 2) and additional material (*17*). *Palaeochersis* shows numerous primitive features present in *Proganochelys* or other nonturtle amniotes, including paired vomers, persistence of supratemporal and interpterygoid vacuities, and epiplastral processes (clavicles). However, the importance of *Palaeochersis* rests in the numerous characters shared with more advanced turtles (Fig. 3), such as the incipient middle ear cavity, the fusion between the pterygoid and the basicranium, and the fusion of the pelvis to the carapace; the latter is thought to be characteristic of pleurodires.

Although identification of a sister group to turtles remains controversial (*18*), *Proganochelys* is considered to be the sister group to all other known turtles (*7, 8, 10, 11*). We performed a cladistic analysis (*19*) of major turtle taxa, using *Proganochelys* as one of the outgroups (Table 1), and only one tree (*20*) was identified (Fig. 3). In this tree, *Palaeochersis* and *Australochelys africanus*, an Early Jurassic turtle from Africa, form a monophyletic assemblage, Australochelidae (*11*). The monophyly of Australochelidae is supported by the presence of large elongated nares (*21*), a nasal platform or bump, a wide occipital plate with depressions for neck muscles, and a temporal fossa that is partially closed by an overhanging flange of the skull roof. The geographic location of both members of Australochelidae suggests a Southern Pangaeic–Gondwanian distribution for the family.

Primitive amniote or chelonian charac-